EDTA 기능화된 산화그래핀/Polyethersulfone(FGO/PES) 나노복합체 멤브레인의 특성 분석 및 중금속과 염료오염 제거

Mehdi Mahmoudian[†], Ehsan Nozad, and Mohammadtaghi Hosseinzadeh

Nanotechnology Research Institute, Urmia University
(2017년 11월 12일 접수, 2017년 12월 21일 수정, 2017년 12월 27일 채택)

Characterization of EDTA Functionalized Graphene Oxide/Polyethersulfone (FGO/PES) Nanocomposite Membrane and Using for Elimination of Heavy Metal and Dye Contaminations

Mehdi Mahmoudian[†], Ehsan Nozad, and Mohammadtaghi Hosseinzadeh

Nanotechnology Research Institute, Urmia University, Urmia, Iran
(Received November 12, 2017; Revised December 21, 2017; Accepted December 27, 2017)

Abstract: In this study, functionalized graphene oxide was prepared by surface grafting of ethylenediaminetetraacetic acid (EDTA) to graphene oxide (GO) surface using ethylenediamine as linking agent and was introduced into polyethersulfone membrane matrix. Grafting of ethylenediaminetetraacetic acid to graphene oxide was confirmed by Fourier transform infrared spectroscopy, scanning electron microscopy, thermogravimetric analysis and X-ray diffraction. The characteristics of prepared nanocomposite membranes were investigated using FESEM and contact angle measurements. The performance of the nanocomposite membranes was investigated in detail for water permeability, salt rejection and protein antifouling test. Also, the performance of membranes in the elimination of several heavy metals and dyes was investigated. The results confirm the significant improvement of hydrophilicity in the modified membranes and a remarkable increase in the salt, heavy metal and dye rejection was achieved.

Keywords: nanocomposite membranes, functionalized graphene oxide, antifouling, surface modification.

Introduction

Membrane technology is a fast growing research area with several applications like desalination and water purification.[1,2] Among the used polymers in membrane fabrication technology, polyethersulfone (PES) has proper film formation property, chemical and mechanical resistant, and miscibility with hydrophilic additives; which made it an appropriate option for many membrane based applications.[3] However, fouling phenomenon under separation condition for the polyethersulfone membranes is caused due to intrinsic hydrophobic property of this polymer.[4] In order to reduce the fouling phenomenon, researchers have investigated several approaches such as surface modification and hydrophilic polymer blending.[5]

Introducing hydrophilic nanoparticles into PES matrix through common blending method has been aroused as one of the most effective strategies to enhance the hydrophilicity of PES membranes.[6,7]

As a new nanostructured material, GO recently has attracted much attention as an additive to enhance the properties of polymer membranes.[8-10] GO can be prepared by the oxidation of graphite. It has a layered structure with oxygen functional groups on its basal planes and edges which makes the GO as a nano material with an ultra-high specific surface area, hydrophilic surface, and negative charged surface.[11] Therefore, many studies show that GO as an additive has a great effect on membrane properties like antifouling and hydrophilicity.[9-12]

However, graphene sheets have some disadvantages for application in membranes. Limited dispersion due to their strong tendency to aggregation causes a decline in permeability and antifouling performances of graphene-incorporated membranes.[13] The entrance of graphene derivatives in mem-

branes may also reduce mechanical strength of membranes, due to weak interaction between graphene and polymer matrix.[14] Therefore, application of modified graphene derivatives with more functional groups and surface charge on the sheets[15-17] can improve the performance of membranes. Additionally, interaction between membrane and foulant can be affected by functionalization. However, there are very few reports on using functionalized GO (FGO) nanostructures on PES membrane properties.[18]

Surface functionalization of GO can be performed by physical wrapping[9] or covalent grafting of species with numerous functional groups.[14]

In this paper, fabrication of a novel nanocomposite membrane by incorporating FGO has been reported. It has been tried to synthesis novel FGO by grafting of EDTA to the surface of GO (GO-EDTA). The existence of hydrophilic moiety on GO surface can enhance surface hydrophilicity, surface charge properties, and as a consequence, membrane antifouling could be improved. To the best of our knowledge, GO-EDTA has not been used to fabricate nanocomposite membranes. Here, the synthesized FGO nanomaterial was blended in the PES matrix dope solution and the phase inversion method was used to fabricate the membrane nanocomposite. The effect of FGO amounts on membranes morphology, hydrophilicity, flux, and antifouling performance were investigated too. FTIR, FESEM and water contact angle analysis were used to investigate the structural properties of prepared membranes. The fouling resistance of the membranes was also analyzed using bovine serum albumin (BSA). The prepared nanocomposite membranes were used for separation of soluble heavy metals (Zn, Cu, Ni and Cd) and dyes like methylene blue (MB) and methyl orange (MO) from water.

Experimental

Materials and Reagents. Polyethersulfone (PES, Mw ~70000) was supplied from BASF. PEG (Mw ~1000), sodium chloride, sodium sulfate, magnesium chloride and EDTA were purchased from Merck. Graphite flakes, sulfuric acid, phosphoric acid, ammonium nitrate, potassium permanganate, bovine serum albumin (BSA, Mw ~67000) and N-methyl-2-pyrrolidone (NMP) were purchased from Sigma-Aldrich.

Preparation of GO. GO was synthesized using graphite flakes by Hummers method.[19] Briefly, 5 g graphite were added gradually to a mixture of 100 mL H_2SO_4 and 12 mL H_3PO_4 along stirring in a cooling bath (ice-water), and then 2.5 g $NaNO_3$ was added drop by drop over 30 min. Finally 20 g $KMnO_4$ was added over 1 h. The resultant mixture was kept in a cooling bath and stirred for about 2 h, following by vigorous stirring for 3 days at ambient temperature. Then, the mixture was diluted with 500 mL of deionized water (DI) slowly, and the excessive $KMnO_4$ was decomposed by H_2O_2 (30 wt%, 15 mL). The solution was centrifuged four times by DI water and then with HCl solution after that, it was washed by DI water for two more times. The resulted precipitated product was dried in oven at 60 °C.

Synthesis of Ethylenediamine Functionalized GO. The reaction between epoxy and carboxylic acid groups on GO with ethylenediamine produces amine functionalize GO (Scheme 1). To this end, briefly, 1.5 g of GO was dispersed in 100 mL ethylenediamine by sonication for 2 h. Then the mixture was kept at 40 °C under stirring condition for 2 h. The FGO was centrifuged and washed with DI water several times.

Synthesis of EDTA Functionalized GO. Amine functionalized GO was dispersed in 55 mL NMP, and 1.8 g EDTA
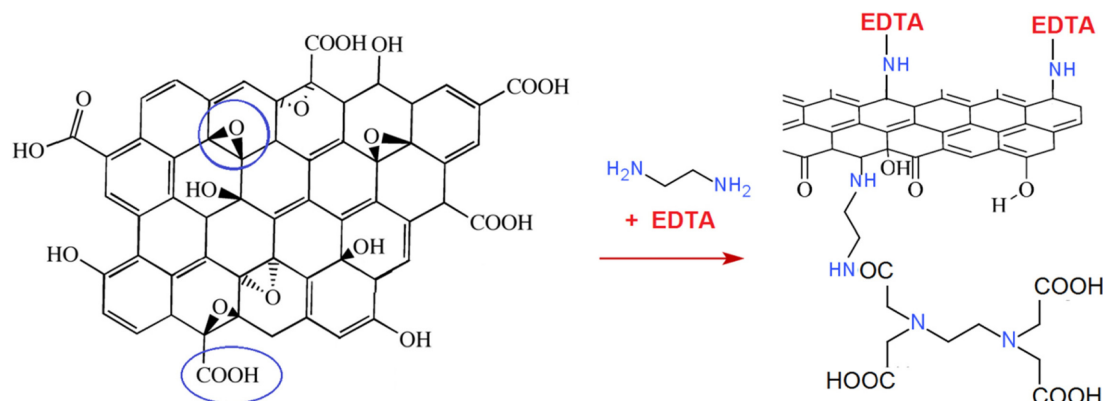
Schem 1. Surface functionalization of graphene oxide with EDTA.

(dissolved in 5 mL water) was added to the mixture. After dispersing the GO, the mixture was refluxed at 80 °C for 24 h. The product was centrifuged and rinsed with DI water and dried in an oven at 60 °C for 24 h. The synthesis process is shown in Scheme 1.

Preparation of Membranes. Classical phase inversion method was used to prepare the membranes using PES and PEG as polymer and pore forming agent material, NMP as solvent, FGO as an additive and distilled water as a nonsolvent coagulation bath. First, FGO (1, 3, 5 and 7 wt% based on the weight of PES) was added into NMP solvent (0.5 g), this solution was then added into the prepared solution of PES and PEG in NMP solvent (Table 1). The resultant solution was then stirred for 24 h at 60 °C. Then, the solution was casted with 250 μm thickness using a knife blade over a clean glass plate. Afterward, the entire assembly was instantly immersed into a water bath at room temperature. Finally, the prepared membranes were washed with distilled water several times and stored at room temperature.

Characterization. Attenuated total reflectance-fourier transform infrared spectroscopy (ATR-FTIR) was used to characterize the surface composition of FGO using an ATR accessory (Bruker IFS-66/S FTIR). Spectra were obtained in the mid-infrared region (400-4000 cm^{-1}).

Hitachi (S4160) field emission scanning electron microscopes (FE-SEM) was used to investigate the cross-section and surface of the membranes. The membranes were chopped into small pieces. These pieces were immersed in liquid nitrogen for 10-15 sec for freezing. Then they were broken down into smaller pieces and were maintained at ambient conditions to get them dried completely. Afterward, the dried samples were gold sputtered to make them electrically conductive. The micrographs were taken under high-vacuum conditions at 20 kV.

The UV-visible spectra of different solutions were monitored on a UV-vis spectrophotometer (CARRY100 Bio 5) for dye concentration detection and fouling tests.

Thermogravimetric analysis (TGA) was measured with a LINSEIS STA TP-1000 thermal analyzer at a heating rate of 15 °C min^{-1}.

Membrane Performance Evaluation. Pure Water Flux (PWF): The PWF of all membranes was measured with a self-fabricated lab scale filtration unit. The membranes were maintained in water for 24 h before conducting the experiment. The membrane samples with 3.6 cm^2 area were placed inside the sample holder. Then, the PWF was measured at 7.5 and 9 bar, consecutively by collecting the filtrated water. For each membrane, average value was obtained from three trials. The PWF was calculated as follow:

$$J_w = \frac{Q}{A\Delta T} \tag{1}$$

where, PWF (J_w) is expressed in unit L/m^{2}h and Q is the quantity of water collected over the initial 5 min of time (ΔT) using a membrane area of A (m^2).

Salt, Heavy Metal and Dye Rejection: Rejection percentage of salt, heavy metal or dye was calculated using the following eq. (2):

$$R\% = \left(1 - \frac{C_p}{C_f}\right) \times 100 \tag{2}$$

Where C_p and C_f are the concentrations (salt, heavy metal or dye) in permeate and the feed, respectively which were measured using a conductometer. Three salts including NaCl, MgSO$_4$ and Na$_2$SO$_4$ were evaluated (salt concentration in the feed was 0.01 molar and the applying pressure was 5 bar). Also, dye rejection tests were performed by methyleneblue and methylorange solutions with initial concentration of 0.005 molar. Additionally, the concentration of dye in permeate was determined by UV spectrophotometer. Furthermore, the heavy metal rejection was determined using aqueous solution of ZnSO$_4$.7H$_2$O (10 ppm), Ni(NO$_3$)$_2$.6H$_2$O (100 ppm), CuSO$_4$.5H$_2$O (1000 ppm) and Cd(NO$_3$)$_2$.4H$_2$O (2500 ppm). Moreover, the concentration of ions in permeate was determined by conductometer.

Antifouling Properties: The antifouling property of the prepared membranes, were determined using, BSA solution in PBS (100 ppm, 50 mM, pH=7) buffer. All membranes were compacted at 6 bar for 30 min. Then the pressure was reduced to 4 bar and PWF of the membrane, J_{w1} (L·m^{-2}·h^{-1}), was determined over a period of 1 min. After completion of the PWF

Table 1. Casting Solution Compositions in Preparion of PES/FGO Membranes

Entry	Casting solution			
	FGO wt%	PES (g)	PEG (g)	NMP (g)
1	0	2	1	7
2	1	2	1	6.98
3	3	2	1	6.94
4	5	2	1	6.90
5	7	2	1	6.86

measurement, BSA solution was loaded inside the permeation cell in order to filter it through the membrane for 30 min. Then the membrane was flushed with pure water for 15 min and PWF J_{w2} (L·m^{-2}·h^{-1}) was measured again. For each membrane, the PWF (J_{w1}) and flux during BSA rejection (J_{w2}) were measured twice. Finally, flux recovery ratio (FRR) was calculated to study the membrane antifouling property as follow:

$$FRR(\%) = \frac{J_{w2}}{J_{w1}} \times 100 \qquad (3)$$

UV-spectrophotometer was used to measure the concentration of BSA in both feed and permeate which all measurements were performed at wavelength of 280 nm. The samples were treated with Bradford reagent and kept for 10 min before measuring their concentrations. Percentage of the BSA rejection was calculated with the following eq. (4):

$$SR\% = \left(1 - \frac{C_p}{C_f}\right) \times 100 \qquad (4)$$

Where C_p (mg/mL) and C_f (mg/mL) are the concentrations of BSA in permeate and the feed, respectively.

Finally, in order to examine biofouling resistance of the membranes, both modified and bare membrane samples were subjected to the static protein absorption test. For this purpose, samples were first ultrasonically treated (100 W, 40 kHz) in phosphate buffer solution (PBS, pH 7.0, 0.1 M) for 5 min, and then incubated in BSA phosphate buffer solution (1.0 mg/mL) at 25 °C for 24 h. PBS was used to wash the samples for several times and then they were treated in PBS under ultrasonication for about 2 min in order to eliminate the surface adsorbed protein. The absorbed protein amounts on the membranes were determined by UV spectroscopy.

Results and Discussion

Characterization of FGO. FTIR: EDTA functionalized GO was synthesized in two stages (Schem. 1). Figure 1 shows the FTIR spectra of GO, GO-ED, GO-EDTA. The characteristic peaks of GO were observed at 1725 cm^{-1} (C=O stretching vibration in carboxylic acid), 1628 cm^{-1} (C=C stretching vibration in aromatic ring), 1230 cm^{-1} (C-O stretching vibration in epoxy), and 1032 cm^{-1} (C-O stretching vibration in alkoxy).[20] For GO-ED samples, a dramatic decrease in the intensities of the peaks at 1720 cm^{-1} and 1032 cm^{-1} was detected compared with pure GO. The appearance of a new peak at 1562 cm^{-1} (N-H bending vibrations) in the spectra of GO-ED samples indi-
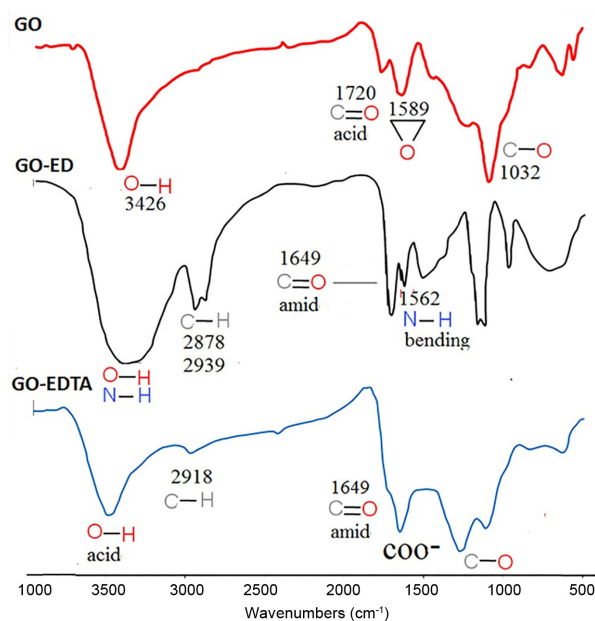

Figure 1. The FTIR spectra of GO, GO-ED, and GO-EDTA.

cated the formation of GO-ED.[21] The strong peak at 3430 cm^{-1} might be related to O-H and N-H stretching vibration. The peaks at 2878 and 2939 cm^{-1} were also strengthened after modification, as ED groups introduce new C-H bonds from methylene groups.[20]

As can be seen in Figure 1 there was some intense changes in GO-ED spectrum after grafting of EDTA. The intensity of broad absorption peak of OH in 3440 cm^{-1} was dramatically weakened after grafting EDTA to GO sheets. The N-H stretching vibrations above 3000 cm^{-1} were weakened and the peak at 1562 cm^{-1} (N-H bending vibrations) was also disappeared after modification. A new strong peak at 1202 cm^{-1} was due to C-O stretching vibration of new COO$^-$ groups from EDTA (due to Zwitter-ionic structure of EDTA). The strong new broad band of 1438-1569 cm^{-1} in GO-EDTA were attributed to the COO$^-$ symmetric and asymmetric stretching vibrations.[22]

Thermo Gravimetric Analysis: TGA was used to investigate both the structure and the thermal stability of graphite, GO, GO-EDTA. The samples were heated from 100 to 900 °C with a heating rate of 15 °C·min^{-1}. As shown in Figure 2(a), GO indicates three weight losses, which the first loss corresponds to the evaporation of moisture and bonded water at 30-150 °C, the second loss is related to deoxygenation of GO at (180-285 °C) generating CO, CO$_2$ and H$_2$O, and the last loss is because of the decomposition of backbone C-C bond at 285-800 °C.[23] GO decomposed at a relatively low temperature of 120 °C, while graphite decomposed at 600 °C. The first

decomposition of GO-EDTA was initiated at higher temperature (160 ℃) with respect to the GO (120 ℃), the second weight loss in GO thermogram was disappeared for GO-EDTA and the main decomposition can be seen at 350-600 ℃ range. The decompositions of GO-EDTA at 160 ℃ were caused by the decomposition of the EDTA groups. Therefore, the FGO showed better thermal stability than GO.

XRD: The XRD patterns of graphite, GO and GO-EDTA were shown in Figure 2(b). As reported usually, the natural graphite reveals a basal reflection (002) peak at 2θ=26.6º.[24] Using Bragg equation, the corresponding d-spacing value of graphite was calculated as d=0.34 nm. However, after oxidation of natural graphite, this peak was moved to 2θ=10.8º, indicating the intercalation of basal plane of the graphite by oxygen functionalities with an interlayer spacing of 0.8 nm.[25,26] A new and less intense peak appeared at 2θ=18-30º in GO samples.

However for GO-EDTA samples, the (002) peak intensity decreased upon the chemical modification of GO, suggesting that EDTA molecules were been attached on the surface of GO. Broadened and less intense peaks emerged at 2θ=13-40º implying that there existed a certain degree of ordered structure usually accompanied by an internal partial regularity of EDTA. Obviously, another peak at 2θ=44º was also observed for GO-EDTA samples which was not present in GO spectrum and confirmed the grafting on the GO layers during the preparation of GO-EDTA samples.

FESEM of GO: Figure 2(c) shows the FESEM images of graphite, GO and GO-EDTA. Graphite sheet was clean, wide, flat and smooth, while GO sheet (Figure 2(c)) exhibited lower width and higher roughness, that provide effective oxidation and intercalation of GO sheets. Roughness increased in GO-EDTA images and revealed the attachment of EDTA groups.

Membrane Characterization and Performance. Membranes were prepared with phase inversion technique with various FGO amounts (1, 3, 5 and 7 wt%) as additives. Functional groups existing on the FGO sheets make an efficient incorporation of this material in polymer casting solution that can give adequate functional groups and surface hydrophilicity on the membranes surface. Also the flat GO sheets might be help-
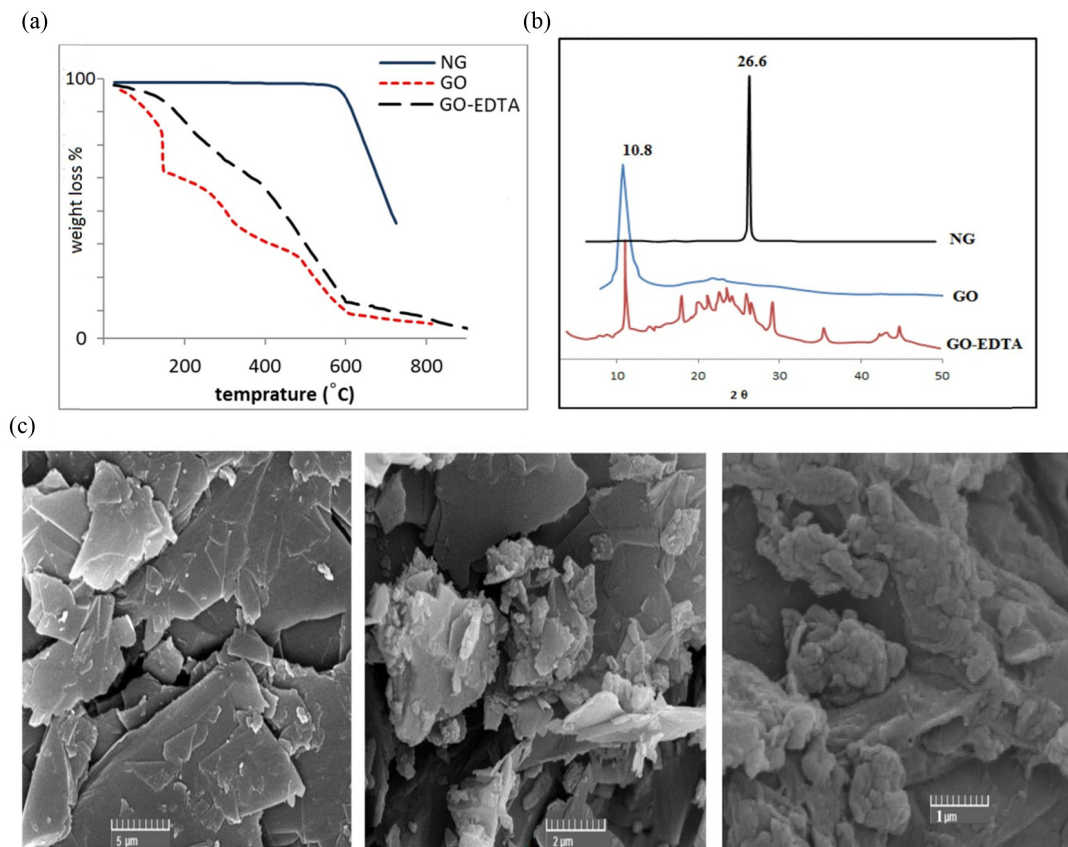
(a)　　　　　　　　　　　　　　　　(b)

(c)

Figure 2. (a) TGA curves of graphite, GO, GO-EDTA; (b) XRD patterns of graphite, GO, GO-EDTA; (c) FESEM images of NG (left), GO (middle) and GO-EDTA (right).

Table 2. Filtration Performance Evaluation Results

Properties evaluated	Membrane sample				
	Neat PES	GO-EDTA (1%)	GO-EDTA (3%)	GO-EDTA (5%)	GO-EDTA (7%)
Water flux at 5 bar (L·m^{-2}·h^{-1})	88.5	217.2	452.4	5.2.7	1105.9
Water flux at 7 bar (L·m^{-2}·h^{-1})	112.6	268.5	552.9	770.8	1298.6
Water flux at 9 bar (L·m^{-2}·h^{-1})	152.8	301.4	703.8	963.8	1625.3
Contact angle (°)	74.3	72.4	69.9	68.3	55.1
BSA adsorption (ppm·cm^{-2})	78.4	72.3	55.2	38.1	21.7
FRR (%)	45.4	82.1	96.1	76.1	25.3
NaCl rejection (%)	45.9	50.0	54.5	53.6	51.5
MgSO$_4$ rejection (%)	52.7	60.5	61.3	59.0	57.0
Na$_2$SO$_4$ rejection (%)	55.0	64.3	68.3	66.0	62.2
MO rejection (%)	66.6	92.4	96.0	92.8	92.2
MB rejection (%)	47.8	54.4	65.8	57.8	56.2
Cu^{2+} rejection (%)	53.1	58.9	86.6	81.1	76.3
Cd^{2+} rejection (%)	50.5	66.1	62.1	69.5	59.3
Ni^{2+} rejection (%)	55.0	74.5	89.1	79.9	73.0
Zn^{2+} rejection (%)	60.0	66.8	96.1	86.3	60.7

ful to the high rejection of solute molecules. To evaluate membrane performance, the effect of FGO amount on membranes morphology, hydrophilicity, flux, antifouling, salt rejection, and dye rejection performance was investigated (Table 2).

PWF of the Membranes: PWF as a key parameter directly reflected the transfer ability of membranes. Figure 3 presented the permeate fluxes of GO-EDTA/PES membranes under the pressures of 5, 7 and 9 bar. As it was expected, the permeate fluxes increased obviously by increasing the trans-membrane pressure for all the membranes. As indicated in Figure 3, the
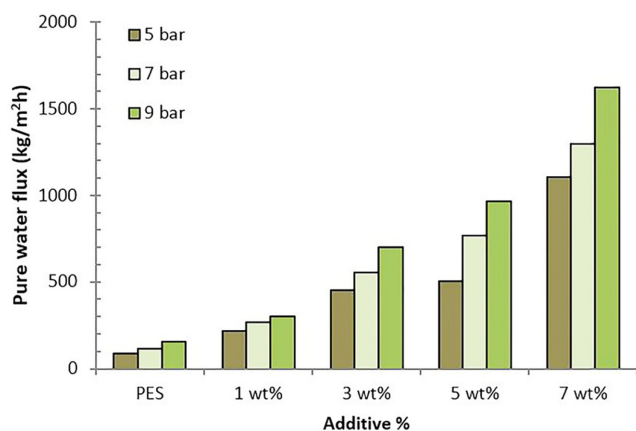

Figure 3. PWF of neat PES and GO-EDTA embedded PES membranes.

additive concentration heavily affected the performance and structure of the membranes. The PWF in membranes is enhanced by increasing of the concentration of GO-EDTA in casting solution. This may be because of this fact that GO-EDTA has improved surface hydrophilicity of membranes and also created larger pores as well as the creation of linear and more finger-like macro-voids in resultant membrane, which started from the top layer and reached to the bottom in higher percentages of the additive, as observed from the cross-sectional FE-SEM images (Figure 4). Commonly, FGO can attract water molecules into the membrane matrix and facilitate their diffusion through the membranes and thus improve the permeability.[27] On the other hand, as it can be seen in FESEM images of membrane surface, by increasing of FGO percent, surface roughness was increased which led to an enhanced water flux as a consequence of increased effective surface area.

FESEM Analysis of Membranes: In order to explore the influence of GO-EDTA as an additive on the morphology of PES membranes, the cross-sectional FESEM images of PES/GO-EDTA membranes with different GO-EDTA contents were investigated. As shown in Figure 4, the prepared nanocomposite membranes had relatively similar macro-void microstructure as the neat PES membrane but the cellular structure of spongy part of modified membranes was different from neat PES. Comparison of membrane containing 1 wt%
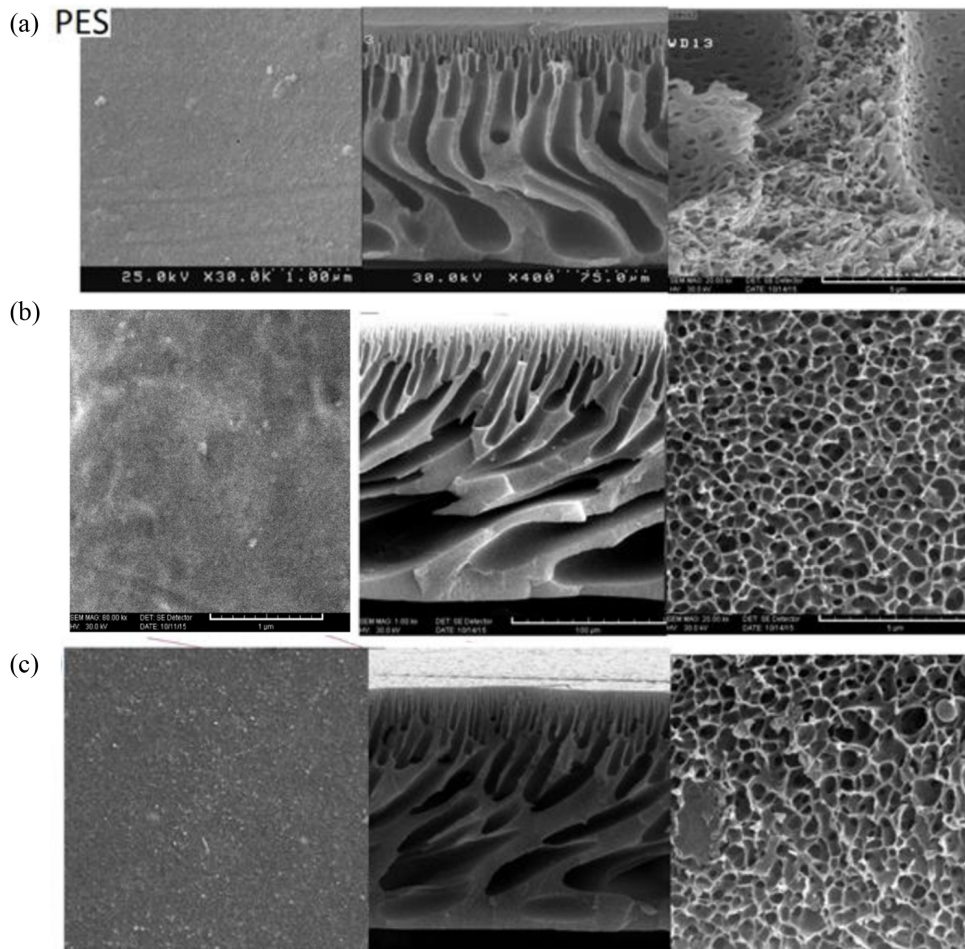
Figure 4. Surface and cross-section FESEM images of the nanocomposite membranes: (a) neat PES; (b) 1 wt% GO-EDTA; (c) 3 wt% GO-EDTA.

GO-EDTA with GO-EDTA 3 wt% membranes revealed that the thickness of the thin top-layer was similar and the porosity of the 3 wt% membrane was a little higher.[28] In the phase inversion process, there were two opposite parameter that played the main role in the formation of macro-voids and channels in membrane structure.[29] These two main parameters were thermodynamic instability of the casting solution which led to instantaneous demixing in the coagulation bath and viscosity of the casting solution. By increasing GO-EDTA content, thermodynamic instability in casting solution increases, which leaded to expansion of macro-voids. Also higher porosity in spongy structure for modified membranes could be related to superior hydrophilic nature of GO-EDTA, which led to much faster migration of PES molecules in precipitation step with water as a non-solvent.

The Hydrophilic/hydrophobic Nature of the Membranes: Contact angle reflected the hydrophilic/hydrophobic nature of

membrane surface which strongly was effective on the adsorption and transmission of permeate molecules. Contact angle values of GO-EDTA/PES membranes were diagramed in Figure 5. In comparison to the neat PES membranes, GO-EDTA/PES membranes displayed lower contact angles due to the presence of hydrophilic functional groups (-OH/-COOH) in FGO. The contact angle values were reduced significantly from 72.4 to 55 with increasing of additive percentage from 1.0 to 7.0 wt%. This observed trend may be due to the accumulation of the hydrophilic FGO nano-sheets on the membrane surface in high amount of the nano-plates.[30] The FGO additive can also increase the roughness of membrane surface (see FESEM images of membrane surface in Figure 4), which enhanced the directional force for droplet spreading through multiple gradients effect.[23]

To study the fouling properties of nanocomposite membranes, the dynamic fouling analysis (flux recovery ratio), and

static fouling analysis (surface protein adsorption) were evaluated for prepared membranes. Static fouling test was performed using a solution of BSA protein (1000 ppm, in an operational pH=7.4, contact time=24 h).

Figure 6 shows the results of static BSA adsorption on the membrane surface. It can be seen that the neat PES membrane had higher amount of BSA adsorption than the nanocomposite membranes due to higher hydrophobicity of the neat PES membranes. In addition, increasing of the FGO percent led to lower BSA adsorption since more additive concentration can increase the hydrophilicity of the membranes as shown by contact angle data. The results of FRR and dynamic fouling for the prepared membranes with and without FGO were shown in Table 2 (Figure 6). Because of higher hydrophilicity of modified membranes, they had higher flux recovery which suggested that protein fouling on membrane layer was more reversible. The highest fouling resistance evaluated by FRR observed for GO-EDTA (3%) sample. It could be related to several parameters such as surface hydrophilicity and roughness. Surface roughness can play a key role due to protein mol-

ecules irreversible deposition into the surface pores.[31] Increasing of the FGO percent improved surface hydrophilicity and, meanwhile, caused higher surface roughness for nanocomposite membranes. Therefore addition of FGO initially to 3 wt% increases FRR, and then, more addition of FGO reduced FRR.

Salt Rejection: Salt rejection performance of prepared nanocomposite membranes was shown in Figure 7. The salt rejection for all samples was in the order of $NaCl < MgSO_4 < Na_2SO_4$. The Effective parameters on salt rejection performance were; size exclusion (steric effects),[32] donnan exclusion (electrical repulsion),[33] concentration polarization[34] and mobility which is determined by diffusion coefficient and effective size of ions.[35] Therefore higher rejection obtained for $MgSO_4$ with respect to NaCl was ascribed to steric effects.[36,37] The
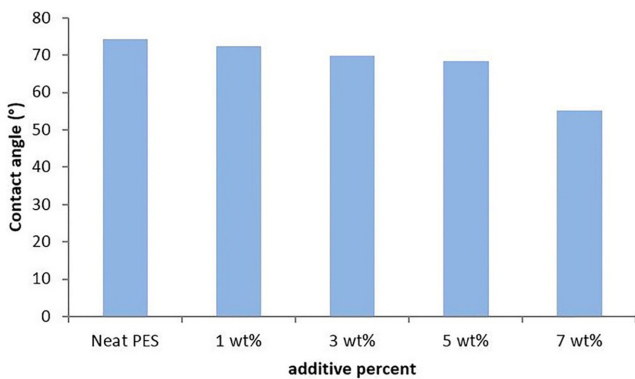
Figure 5. Water contact angle of the prepared membranes.
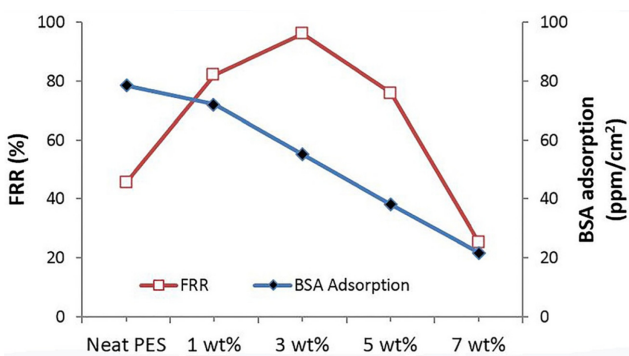
Figure 6. Water flux recovery ratio and BSA adsorption of the membranes with the different concentrations of FGO.
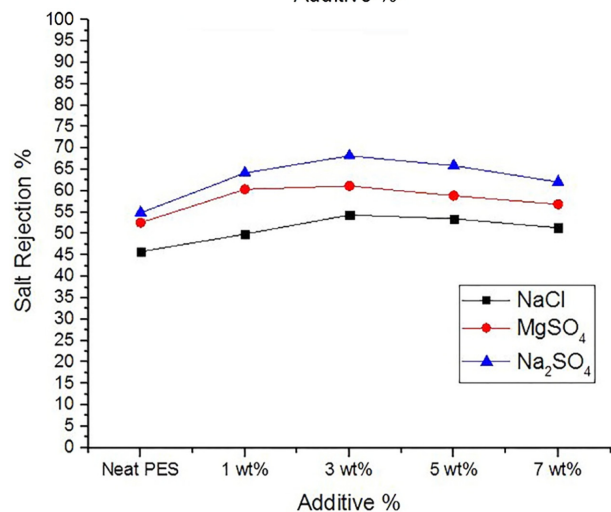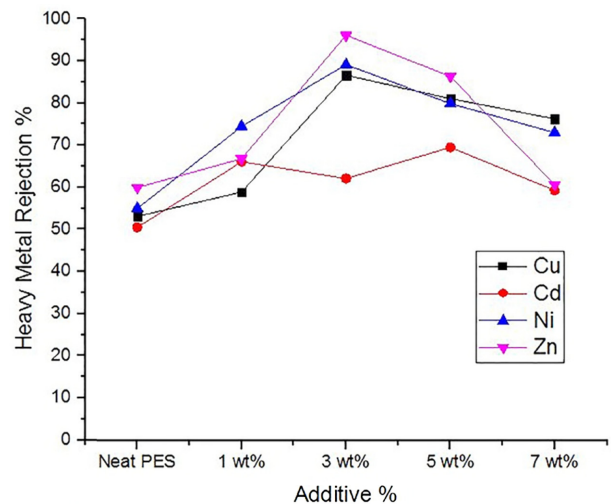
Figure 7. Salt and heavy metal rejection performance of the prepared membranes.

membrane surface has negative surface charge distribution due to the carboxylate groups on the membrane surface, which adsorbed cations from the solution and repeled anions.[35] The positive ions with higher charge covered the surface negative charge and results in more negative ions passed through membrane pores. Therefore the Na_2SO_4 with monovalent positive ion showed higher rejection rate than $MgSO_4$ with divalent positive ion. The rejection performance of all the modified membranes was more than neat PES membrane. Increasing of FGO concentration from 1 to 3 wt% improved salt rejection but higher amount of FGO, decreased salt rejection slightly. This may be because of the increase in surface negative charge caused by FGO to 3%, on the other hand, more amount of FGO increased the pore diameter of membrane and reduced removal efficiency.

Heavy Metal Removal: The separation of heavy metal ions by membrane was achieved by both size exclusion and electrical interactions between the ions in the feed and the nanocomposite membranes. The modified membranes had an amphoteric behavior in contact with the aqueous solutions due to the formation of the ammonium ($-NH_3^+$) and carboxylate ($-COO^-$) groups.[38] The degree of ionization of these functional groups was a function of the solution pH. To increase the rejection of positive heavy metal ions, the pH should be in neutral or basic condition to have negative membrane surface charge and therefore the absorption capacity of membrane toward metal ion will be increased.

Figure 7 showed the obtained heavy metal rejection values of Cd(II), Cu(II), Ni(II), and Zn(II) ions for FGO modified membranes. The rejection percent of heavy metals was improved by using FGO in PES membranes. The rejection percent for heavy metals didn't show an ordered trend but it seemed that it followed this manner which rejection for Ni^{2+} and Zn^{2+} was higher than the others. This was not related to the hydrated ionic radius as Ni^{2+}(4.04 Å)$<Cu^{2+}$(4.19 Å)$<Cd^{2+}$(4.26 Å)$<Zn^{2+}$(4.3 Å).[39,40] Affinity between EDTA groups and ions maybe caused this trend. Like salt rejection results, the highest ion removal was observed for mixed matrix membrane containing 3% FGO. This phenomenon can be explained by the balance between pore size, surface roughness and surface charge.

Dye Removal: In the current study, filtration performance of the prepared membranes was investigated by the removal efficiency of MB and MO organic dyes (Figure 8). Figure 9 showed the obtained dye rejection values for prepared membranes. As can be seen, the retention of MO was more than

MB for all of the prepared membranes. Additionally, the rejection performance of nanocomposite membranes was more than neat PES membrane that confirmed the better filtration performance of the prepared mixed matrix membranes. Repulsion effect between the negative surface of membrane and negatively charged dye molecules can be the main reason of the higher performance of the blended membranes.[23] In neutral pH, MO had a negative charge because of dissociation of sulfonic groups (see Figure 8). Also, the prepared blended membranes had negative charge due to the presence of several acidic functional groups on the FGO sheets.[41] Increase in FGO additive concentration from 1 to 3 wt% improved dye removal but higher amount of FGO decreased removal efficiency slightly. This may be due to increasing surface negative charge by FGO to 3% but more percent of FGO increased the pore diameter of membrane and reduced removal efficiency. The results were in agreement with salt rejection data and heavy metal removal and the highest dye removal was observed for the sample with 3% FGO additive concentration.
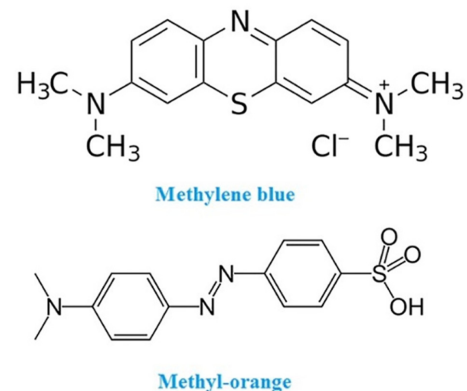

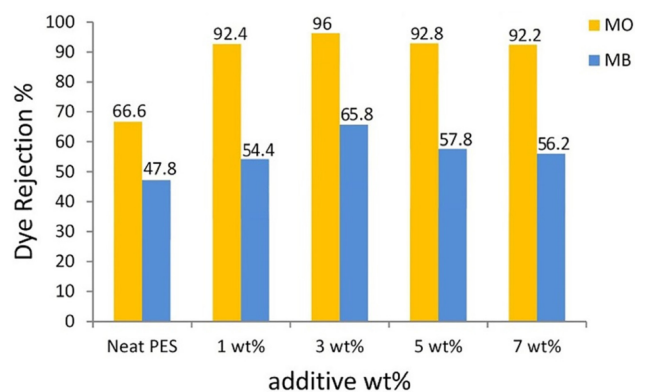**Figure 8.** The molecular structure of the studied dyes.

Figure 9. Dye rejection performance of the prepared membranes.

Table 3. Physical Properties of Membranes

Sample	BET specific surface area $(m^2 \cdot g^{-1})$	Pore volume $(cm^3 \cdot g^{-1})$	Pore diameter (nm)
PES	25.67	0.02	5.50[39]
PES/FGO (1%)	49.5	0.06	2.44
PES/FGO (3%)	48.69	0.07	3.33
PES/FGO (3%)[a]	47.3	0.07	3.33

[a]The BET test was performed under pressure (10 bar).

Figure 10. The BET and BJH plot (pore size distribution) of membranes.

Table 3 lists the BET surface area, pore diameter and pore volume of the PES/FGO membranes. From these results, as expected, a higher surface area for the mixed matrix membrane was obtained; in particular the BET surface area was equal to 49.5 and 48.69 kg/m² for the PES/FGO (1%) and PES/FGO (3%) respectively. The incorporation of FGO nano-platelets in the polymer matrix modifies the pore volume of the polymeric membrane too. The pore size distributions (BJH-Plot) for FGO containing membranes were shown in Figure 10. The results showed that the changing of FGO percent from 1 to 3% had minor effect on the pore size distribution of the membranes and a slight increase could be observed by increasing FGO percent. Most of the pore sizes were less than 5 nm, revealing that the membranes are in the meso-porous domain. Also the BET plot was V type that is characteristic of meso-porous material. The average pore diameter and pore volume for PES/FGO (1%) was 2.44 nm and 0.06 cm³·g⁻¹. Also pore diameter and pore volume for PES/FGO (3%) were 3.33 nm and 0.07 cm³·g⁻¹, respectively, which showed that, increasing FGO influenced the pore formation of the membranes. To evaluate the effect of pressure on membrane mechanical properties the
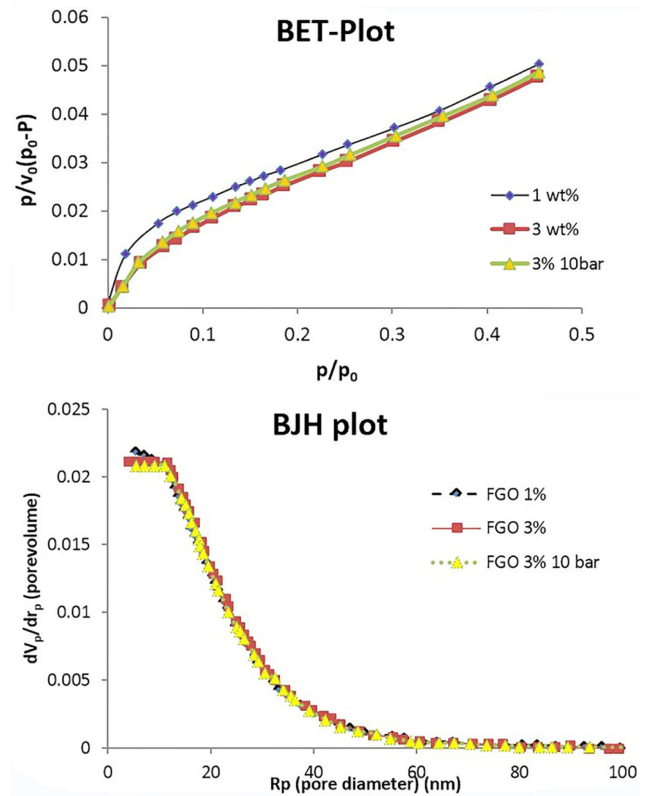
BET data was taken at 10 bar pressure for PES/FGO (3%). The results showed that membrane has enough mechanical strength and the pore volume and diameter didn't changes under pressure remarkably.

The results obtained in this study were compared to the previous scientific literature in which GO has been used to modify PES as presented in Table 4.[39,41,43-45] As it can be seen, the

Table 4. The Results of Other Researchers in Modification of PES Membranes by GO and FGO

Polymer/Additive (wt%)	Water flux $(kg \cdot m^{-2} \cdot h^{-1})$	Contact angle change (°)	FRR (%) improvement	Pore diameter (nm)	Reference
PES/FGO 3%	88.5→452 (0.5 MPa)[a,b]	74.3→69.9	45.4→96.1	3.33	This work
PES 17%/GO 1%	27→45 (0.4 MPa)	64→51	78→91	-	[27]
PES/GO-Ly 1.5%	198→318.0	83.5→65.5	-	-	[40]
PES 21%/TiO₂/GO 0.15%	23.1→ 45.0 (0.5 MPa)	65.5→55.5	75→94%	3.99→4.74	[41]
PES/GO 1%	30→37.5 (500 kPa)	70.8→61.2	63→50%	2.09→2.76	[27]
PES/rGO/Ag 0.2%	429.8	63→53.2	48.3→67.2	7.72→10.44	[42]
PES/PVP/FGO 5% FGO	197.4 →153.5	85.5→63.1	86.6→ 92.1	35.9→36.4	[42]
PES/PVP/GO 0.1% GO	8.2→13.5 (0.4 MPa)	65.2→55.3	35→75	3.2→3.8	[38]

[a]Applied pressure. [b]The changes of neat polyethersulfone properties to nanocomposite membrane are shown by (→).

higher water flux was seen in this work for the sample containing 3% FGO than previous works. Moreover the FRR% was 96.1% in this work that was also better than previous reported results. The other results were relatively similar to previously reported works.

Conclusions

PES/FGO nanocomposite membranes were prepared via classical phase inversion method by dispersing of GO-EDTA nanosheets in the PES casting solution. GO-EDTA was prepared via direct interaction of previously amine functionalized GO sheets with carboxylic acid groups of EDTA. The FESEM analyses showed that the addition of EDTA-GO nanosheets improved the microstructure of the PES membranes. The nanocomposite membranes exhibited improved hydrophilic, water flux, antifouling and mechanical properties. The addition of GO-EDTA also improves the rejection of salt, heavy metal and dyes more efficient than neat PES. The mechanical properties of membranes were also improved using FGO as revealed by BET.

References

1. T. Tsuru, *Membr. Technol.*, **2016**(3), 7 (2016).
2. W. Luo, H. V Phan, M. Xie, F. I. Hai, W. E. Price, M. Elimelech, and L. D. Nghiem, *Water Res.*, **109**, 122 (2017).
3. B. Khorshidi, J. Hajinasiri, G. Ma, S. Bhattacharjee, and M. Sadrzadeh, *J. Membr. Sci.*, **500**, 151 (2016).
4. S. C. Chen, G. L. Amy, and T.-S. Chung, *Water Res.*, **88**, 144 (2016).
5. J. Lin, W. Ye, K. Zhong, J. Shen, N. Jullok, A. Sotto, and B. Van der Bruggen, *Chem. Eng. Process. Process Intensif.*, **107**, 194 (2016).
6. O. T. Mahlangu, R. Nackaerts, J. M. Thwala, B. B. Mamba, and A. R. D. Verliefde, *J. Membr. Sci.*, **524**, 43 (2017).
7. W. Fu, C. Carbrello, X. Wu, and W. Zhang, *Nanoscale*, **9**, 15550 (2017).
8. L. Wang, N. Wang, J. Li, J. Li, W. Bian, and S. Ji, *Sep. Purif. Technol.*, **160**, 123 (2016).
9. N. Ghaemi, S. Zereshki, and S. Heidari, *Process Saf. Environ. Prot.*, **111**, 475 (2017).
10. E. Igbinigun, Y. Fennell, R. Malaisamy, K. L. Jones, and V. Morris, *J. Membr. Sci.*, **514**, 518 (2016).
11. R. P. Pandey, G. Shukla, M. Manohar, and V. K. Shahi, *Adv. Colloid Interface Sci.*, **240**, 15 (2017).
12. S.-S. Li, Y. Xie, T. Xiang, L. Ma, C. He, S. Sun, and C.-S. Zhao, *J. Membr. Sci.*, **498**, 135 (2016).
13. Y. Oh, D. L. Armstrong, C. Finnerty, S. Zheng, M. Hu, A. Torrents, and B. Mi, *J. Membr. Sci.*, **541**, 235 (2017).
14. J.-K. Wu, C.-C. Ye, T. Liu, Q.-F. An, Y.-H. Song, K.-R. Lee, W.-S. Hung, and C.-J. Gao, *Mater. Des.*, **119**, 38 (2017).
15. M. G. Kochameshki, A. Marjani, M. Mahmoudian, and K. Farhadi, *Chem. Eng. J.*, **206**, 309 (2017).
16. J. U. Lee, W. Lee, J. W. Yi, S. S. Yoon, S. B. Lee, B. M. Jung, B. S. Kim, and J. H. Byun, *J. Mater. Chem. A*, **12893**, 1 (2013).
17. J. Yan, G. Chen, J. Cao, W. Yang, B. Xie, and M. Yang, *New Carbon Mater.*, **370**, 27 (2012).
18. J. Zhu, M. Tian, J. Hou, J. Wang, J. Lin, Y. Zhang, J. Liu, and B. Van der Bruggen, *J. Mater. Chem. A*, **4**, 1980 (2016).
19. N. M. S. Hidayah, W. W. Liu, W. L. Chin, N. Z. Noriman, and U. Hashim, *Adv. Mater. Res.*, **1133**, 476 (2016).
20. J. Yan, G. Chen, J. Cao, W. Yang, B. Xie, and M. Yang, *Carbon N. Y.*, **52**, 624 (2013).
21. B. Xue, J. Zhu, N. Liu, and Y. Li, *Catal. Commun.*, **64**, 105 (2015).
22. C. Zhao, L. Ma, J. You, F. Qu, and R. D. Priestley, *Desalin. Water Treat.*, **57**, 8942 (2016).
23. S. Yuan, J. Zhang, Z. Yang, S. Tang, B. Liang, and S. O. Pehkonen, *New J. Chem.*, **41**, 6475 (2017).
24. T. Chen, J. Qiu, K. Zhu, X. He, X. Kang, and E. Dong, *Mater. Lett.*, **128**, 19 (2014).
25. M. Kotal, S. S. Banerjee, and A. K. Bhowmick, *Polymer*, **82**, 121 (2016).
26. S. Miao, H. Zhang, X. Li, and Y. Wu, *Int. J. Hydrogen Energy*, **41**, 331 (2016).
27. N. Abdullah, R. J. Gohari, N. Yusof, A. F. Ismail, J. Juhana, W. J. Lau, and T. Matsuura, *Chem. Eng. J.*, **289**, 28 (2016).
28. W. Shao, S. Wu, Z. Hong, Q. Wang, Y. Xiong, R. Yi, Q. Xie, and Z. Xiao, *J. Appl. Polym. Sci.*, **133**, 43769 (2016).
29. S. Zinadini, V. Vatanpour, A. A. Zinatizadeh, M. Rahimi, Z. Rahimi, and M. Kian, *J. Water Process Eng.*, **7**, 280 (2015).
30. S. A. Kiran, Y. L. Thuyavan, G. Arthanareeswaran, T. Matsuura, and A. F. Ismail, *Chem. Eng. J.*, **286**, 528 (2016).
31. H. M. Hegab and L. Zou, *J. Membr. Sci.*, **484**, 95 (2015).
32. M. E. A. Ali, L. Wang, X. Wang, and X. Feng, *Desalination*, **386**, 67 (2016).
33. A. Ghaee, M. Shariaty-Niassar, J. Barzin, T. Matsuura, and A. F. Ismail, *Desalin. Water Treat.*, **57**, 14453 (2016).
34. P. H. H. Duong, S. P. Nunes, and T.-S. Chung, *J. Membr. Sci.*, **520**, 840 (2016).
35. P. Daraei, N. Ghaemi, and H. S. Ghari, *Cellulose*, **24**, 915 (2017).
36. R. Ling, L. Yu, T. P. T. Pham, J. Shao, J. P. Chen, and M. Reinhard, *J. Membr. Sci.*, **524**, 529 (2017).
37. A. Sabir, W. Falath, K. I. Jacob, M. Shafiq, M. A. Munawar, A. Islam, N. Gull, M. T. Z. Butt, K. Sanaullah, and T. Jamil, *Eur. Polym. J.*, **85**, 266 (2016).
38. C.-V. Gherasim and P. Mikulášek, *Desalination*, **343**, 67 (2014).
39. S. S. Metwally and R. R. Ayoub, *Appl. Clay Sci.*, **126**, 33 (2016).

40. P. Kabwadza-Corner, M. W. Munthali, E. Johan, and N. Matsue, *Am. J. Anal. Chem*., **5**, 395 (2014).

41. S. Zinadini, A. A. Zinatizadeh, M. Rahimi, V. Vatanpour, and H. Zangeneh, *J. Membr. Sci*., **453**, 292 (2014).

42. X. Zhang, C. Cheng, J. Zhao, L. Ma, S. Sun, and C. Zhao, *Chem. Eng. J*., **215**, 72 (2013).

43. L. Duan, Y. Wang, Y. Zhang, and J. Liu, *Appl. Surf. Sci*., **355**, 436 (2015).

44. M. Safarpour, V. Vatanpour, and A. Khataee, *Desalination*, **393**, 65 (2016).

45. V. Vatanpour, A. Shockravi, H. Zarrabi, Z. Nikjavan, and A. Javadi, *J. Ind. Eng. Chem*., **30**, 342 (2015).